https://doi.org/10.5194/egusphere-2024-1800
Preprint. Discussion started: 15 July 2024

Title:

Enhancing environmental models with a new downscaling method for global radiation in complex terrain

Authors / co authors:

Druel, Arsène[1], Ruffault, Julien[1], Davi, Hendrik[1], Chanzy, André[2], Marloie, Olivier[1], De Cáceres, Miquel[3], Mouillot, Florent[4], François, Christophe[5], Soudani, Kamel[5], and Martin-StPaul, Nicolas K.[1].

[1] URFM, INRAE, 84000 Avignon, France; [2] UMR 1114 EMMAH, INRAE, Avignon University, 84000 Avignon, France; [3] CREAF, Centre de Recerca Ecològica i Aplicacions Forestals, Bellaterra, Catalonia, Spain; [4] UMR 5175 CEFE, Montpellier University, CNRS, EPHE, IRD, Montpellier, France; [5] UMR 8079 ESE, UPS, CNRS, AgroParisTech, Orsay, France

Correspondence email: arsene.druel@inrae.fr

https://doi.org/10.5194/egusphere-2024-1800
Preprint. Discussion started: 15 July 2024

Abstract:

Global radiation is a key climate input in forest process-based models (PBM) as it determines photosynthesis, transpiration and the canopy energy balance. While radiation is highly variable at fine spatial resolution in complex terrain due to shadowing effects, data required for PBM currently available over large extents are generally at spatial resolution coarser than ~9 km. Downscaling radiation from large-scale to high resolution available from digital elevation models is therefore of potential importance to refine global radiation estimates and improve PBM estimations. In this study, we introduce a new downscaling model that aims to refine sub-daily global radiation data obtained from climate reanalysis or projection at large scales to the resolution of a given digital elevation model. First, downscaling involves splitting radiation into direct and diffuse fraction. Then, the influence of surrounding mountains' shade on direct radiation and the "bowl" (deep valley) effect on diffuse radiation is considered. The model was evaluated by comparing simulated and observed radiation at the Mont Ventoux mountain study site (southeast of France) using the recent ERA5-Land hourly data available at 9 km resolution as input and downscaled at different spatial resolution (from 1 km to 30 m resolution) using a digital elevation model. The downscaling algorithm improved the reliability of radiation at the study site in particular at scales below 150 m. Finally, by using two different process based models (Castanea, a process-based model simulating tree growth, and SurEau, a plant-hydraulic model simulating hydraulic failure risk), we showed that accounting for fine resolution radiation can have a great impact on predictions of forest functions and climatic risks.

short summary:

Accurate radiation data are essential for understanding ecosystem growth. Traditional large-scale data lack the precision needed for complex terrains, e.g. mountainous regions. This study introduces a new model to enhance radiation data resolution using elevation maps, which accounts for sub-daily direct and diffuse radiation effects caused by terrain features. Tested on Mont Ventoux, this method significantly improves radiation estimates, benefiting forest growth and climate risk models.

https://doi.org/10.5194/egusphere-2024-1800
Preprint. Discussion started: 15 July 2024

1. INTRODUCTION

Studies assessing the impacts of climate change on forest ecosystem functions increasingly rely on high resolution spatial and temporal climate data. For example, process-based models that aim to evaluate the effect of climate on forest functions and services require daily or sub-daily temporal resolution meteorology as input (*e.g.*, Davi et al., 2006; De Cáceres et al., 2023; Granier et al., 2007; Ruffault et al., 2013, 2022, 2023) to simulate key ecophysiological processes (transpiration, photosynthesis or water potential). Yet, even relatively fine-grained (*i.e.*, 1 km) historical or projected climate products (Hijmans et al., 2005; Brun et al., 2022) do not correspond to the "topographic scale" and cannot reproduce fine-scale patterns observed in heterogeneous landscapes. Moreover, employing spatially-coarse climatic projections can lead to biassed and irrelevant inferences of local ecological patterns (Bedia et al., 2013) or to substantial errors in impact studies (e.g., Patsiou et al., 2014; Randin et al., 2009). Improving methodologies to provide climatic data at high spatio-temporal resolution variation is therefore crucial to better understand and forecast the spatial heterogeneity in forest structure and functions.

Among climate variables, radiation is a key driver of plant functioning and productivity globally (Churkina and Running, 1998) though two main mechanisms. On one hand, global radiation determines the photosynthetically active radiation (PAR), *i.e.*, the available energy for photosynthesis and thus plant productivity. Numerous studies have shown the relationship between the amount of solar radiation and the distribution of plant species or communities worldwide (Dirnbock et al., 2003; Franklin, 1998; Meentemeyer et al., 2001; Tappeiner et al., 1998; Zimmermann and Kienast, 1999). On the other hand, the radiation reaching a vegetation surface is an important component of the canopy energy balance, driving surface temperature and vapour pressure deficit (Monteith, 1981). Radiation is thus a key driver of evapotranspiration which enters in most potential evapotranspiration formulations (Fisher et al., 2011) and water balance models (Granier 1999; Ruffault et al. 2013; De Cáceres et al., 2015). Through its effect on leaf-temperature and vapour pressure deficit, radiation also influences the water-status of the leaves which in turn will drive many plant functions including growth, stomatal aperture and desiccation (Martin-StPaul et al., 2023).

In regions with a complex orography, climatic variations can occur over distances ranging from a few metres to a few kilometres. This phenomenon, referred to as topoclimate (Bramer et al., 2018), can play a crucial role in shaping flora and fauna habitat as well as a multitude of ecosystem processes related to climatic variability (Austin, 2002; Piedallu & Gégout,

https://doi.org/10.5194/egusphere-2024-1800
Preprint. Discussion started: 15 July 2024

2008; Randin et al., 2009). Accounting for topographic effects on spatial radiation patterns has been well studied with the purpose, for instance, of improving niche models in mountainous areas (Piedallu & Gégout, 2008; Randin et al., 2009). So far, such radiation data are measured or computed from local meteorological stations, or from coarse-scale global meteorological products such as reanalyses (e.g. De Cáceres et al., 2018).

Direct radiation is a primary driver of topoclimate variations, as it can undergo changes at a very local scale due to several processes. At the scale of a massif, the surrounding topography can cast shadows on a given point because the sun rays can be physically interrupted. In other words, the presence of nearby high peaks will impact the rays directly coming from the sun. At the scale of a point in space, the slope and aspect, will in addition modify the direct radiation intensity received. In the northern hemisphere, a south face will receive more radiation than a north face, and this will be modulated by the angle between the sun rays and the slope at the point. Similarly, the surrounding topography will affect diffuse luminosity (*e.g.*, on cloudy days) anisotropically (at 360°), leading to lower luminosity in valley bottoms (*i.e.*, the “bowl effect”).

Historically, the primary method for accounting for the effects of topography on radiation has been to rely on slope or aspect. Indeed, these parameters are relatively simple to measure (e.g., through GIS) and the global radiation flux at the surface can be easily derived from those (Austin et al., 1990; Carroll et al., 1999; Clark et al., 1999; Pierce et al., 2005). However, this downscaling approach overlooks a significant portion of the processes involved in radiation attenuation due to sky obstruction by surrounding topography. Regional climate models (RCMs), on the other hand, calculate radiation by accounting for atmospheric processes in relation to land-surface processes (energy balance etc…). Nevertheless, they typically operate on fixed grids, usually at scales of several kilometres (Bailey et al., 2023), which is not precise enough for operational use at point level. More recently, another method employed is statistical downscaling, which is empirical and based on regressions (Davy & Kusch, 2021; Fealy & Sweeney, 2008) or machine learning techniques (Hernanz et al., 2023). However, this requires a lot of field data in different contexts to elaborate an empirical model.

Piedallu & Gégout (2008) proposed one method using the slope and the aspect of the point to compute the sun intensity and taking into account the surrounding topography to compute radiation accounting for direct shadowing. They produced a fine scale map (50 * 50 m) over France which is dedicated to statistical niche modelling or mortality risk assessment (Piedallu & Gégout, 2008). However, in the case of process-based vegetation models this

https://doi.org/10.5194/egusphere-2024-1800
Preprint. Discussion started: 15 July 2024

has several limitations. Firstly, their approach relies on interpolated meteorological station data to compute the radiation correction at a monthly time step and is thus limited in terms of temporal and spatial accuracy, leading to significant biases in vegetation growth or the smoothing of climatic extremes. Secondly, they do not separate diffuse and direct radiation using clouds but only use an empirical correction of the total radiation using cloud cover. Finally, the “bowl effect” on diffuse radiation is not taken into account. This method based on measurements is thus limited for projection purposes and requires a large network of equipped stations, resulting in uncertainty. Moreover, it has been applied only to France and has not been generalised to other regions or periods.

In this study we present a process-based method to downscale coarse resolution (0.1° at best in general) global radiation data (such as global reanalysis or climate projections) made on flat surfaces down to the level of 1 km to 30 m resolution Digital Elevation Model (DEM) by accounting for slope, aspect and the shadowing effect on direct radiation and for the bowl effect on diffuse radiation. The method can be applied at any resolution, depending on the choice of the DEM. Moreover, it relies on any type of radiation data, making it applicable to any region in the world and to historical periods as well as future projections. The possibility to use reanalyses-derived radiation furthermore ensures physical consistency between the different climate variables used in process-based models. The algorithm was tested on the Mont Ventoux and compared with PAR measurements recorded during 2 years at 7 sites on this complex topographic area. Finally we evaluated how this new radiation product can impact ecological patterns by simulating the gross primary productivity (GPP) and the risk of hydraulic failure for *Fagus sylvatica* using two process-based models.

2. METHODS

2.1. Radiation downscaling model

The proposed radiation downscaling model aims to refine sub-daily global radiation data obtained from reanalysis at large scales to the resolution of a given DEM. This process-based method can be adapted depending on the input dataset and accounts for the shadowing effect on direct radiation and the bowl effect on diffuse radiation. In order to ensure its versatility and applicability, we reduced the need for external data that can be challenging to obtain at the local scale, such as cloudiness (Dubayah and Loechel, 1997; Piedallu and Gégout, 2007). The only required input is a DEM whose resolution must match the desired final spatial resolution of the radiation data.

Our methodology involves four distinct steps, outlined as follows (see Fig. 1 for

https://doi.org/10.5194/egusphere-2024-1800
Preprint. Discussion started: 15 July 2024

visualisation):

i. Splitting direct and diffuse radiation from a large-scale global radiation dataset (optional if the data already contain direct and diffuse radiation).

ii. Downscaling direct radiation by considering local topography and shadowing effects.

iii. Downscaling diffuse radiation by estimating the proportion of diffuse radiation that reaches the target point relative to the surrounding topography.

iv. Summing the downscaled direct and diffuse radiation components.

These steps are described in detail in the subsequent sections.

https://doi.org/10.5194/egusphere-2024-1800
Preprint. Discussion started: 15 July 2024

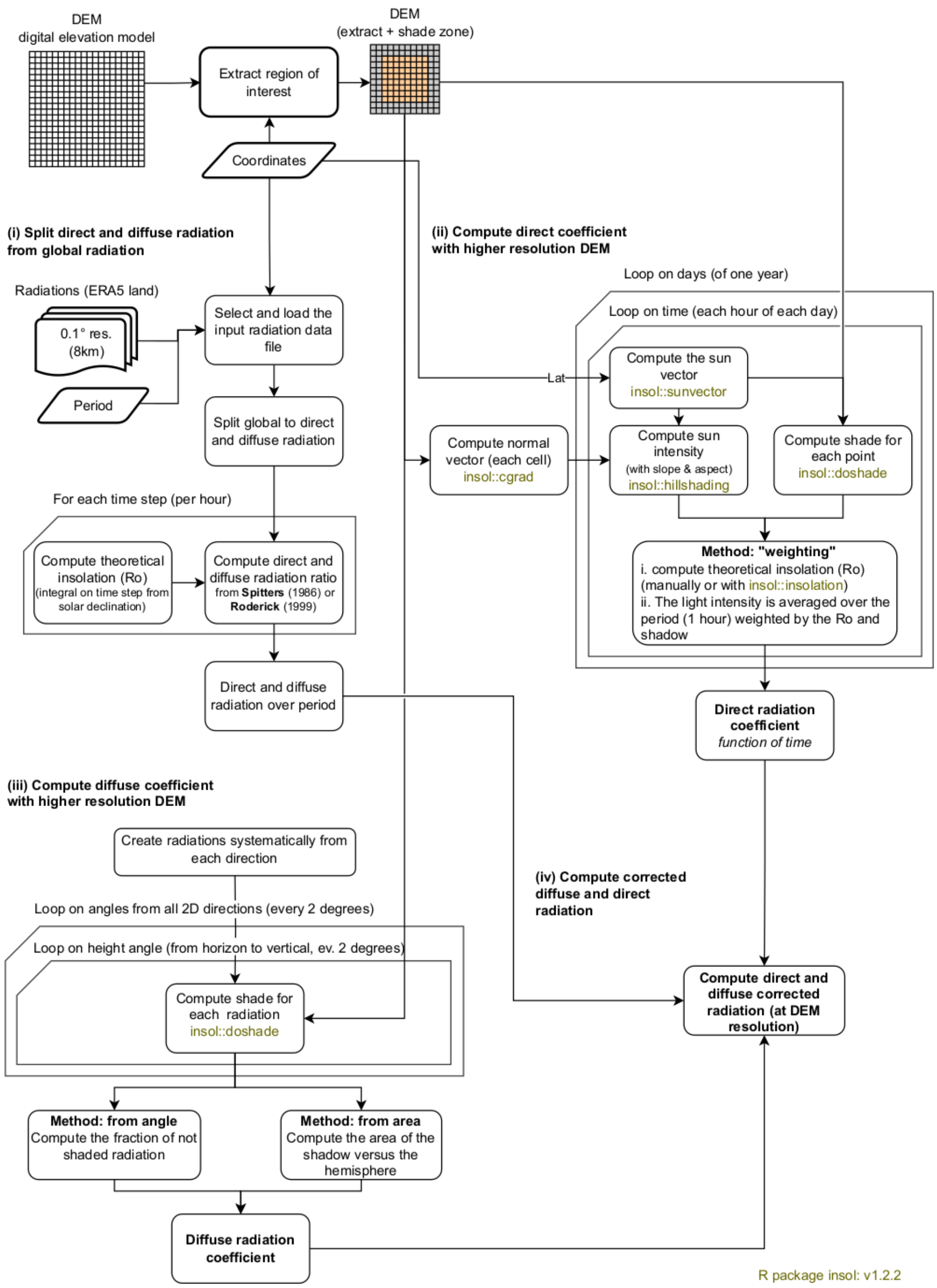

Figure 1: Simplified workflow of radiation downscaling, showing the four different steps of the procedure. The bold boxes at the top left show the data required as inputs (DEM, coordinates, period and large scale radiation), the green boxes show the functions of the external R package used (insol), the truncated boxes show the loops and the rounded boxes show the various stages.

https://doi.org/10.5194/egusphere-2024-1800
Preprint. Discussion started: 15 July 2024

2.1.1. Splitting direct and diffuse radiation

In cases where only global radiation is available from the input dataset, as in products like ERA5-Land (Muñoz-Sabater et al., 2021), a first step involves extracting hourly direct and diffuse radiation (Fig. 1.i). Various methods exist for this purpose (Oliphant & Stoy, 2018). In this study, we adopted the approach proposed by Spitters et al. (1986). This choice was driven by the relative simplicity of this approach and the fact that it was originally developed for European landscapes. Additionally, we explored other methods, such as the one proposed by Roderick (1999) and the one proposed by Bird and Hulstrom (1981). Results obtained using the Roderick (1999) method align consistently with those presented herein (results not displayed). Unlike the method by Spitters et al. (1986), the method by Bird and Hulstrom (1981) does not rely on global radiation values but instead aims to derive the values of direct and diffuse radiation from theoretical radiation, temperature, humidity, among other factors. However, the outcomes generated by this model significantly deviated from those obtained using the Spitters et al. (1986) method and exhibited inconsistency with available measurements (not shown).

The method of Spitters et al. (1986) that was used in this study is an empirical computation technique based on the ratio between theoretical extraterrestrial irradiance (R_0) and the observed value of global radiation (R_g). Specifically, it operates on the assumption that as the ratio of R_g to R_0 decreases, the proportion of diffuse radiation (R_{difl}) relative to direct radiation (R_{dir}) increases - an effect attributed to cloud cover.

To compute R_0 (in J.m^{-2}.s^{-1}), a common physically-based approach involves using the radiation incident on a plane parallel to the Earth's surface and the sine of solar elevation (which is dependent on latitude and solar time), as follows:

a. $R_0 = R_{sc}\left[1 + 0.033 \times \cos\left(doy \times 360/365\right)\right] \times \sin(\beta)$

b. $\sin(\beta) = \sin(\lambda) \times \sin(\delta) + \cos(\lambda) \times \cos(\delta) \times \cos\left(15 \times (t_h - 12)\right)$ (1)

c. $\delta = \dfrac{\pi \times 23.45}{180} \times \sin\left(2 \times \pi \times \dfrac{doy + 284}{365}\right)$

With R_{sc} representing the solar constant (1 370 J.m^{-2}.s^{-1}, I.E.A., 1978), *doy* the day of the year, sin(β) the sine of the solar elevation angle, λ the latitude of the site (in radian), δ the solar declination angle (in degrees) approximated using the Fletcher method as described in Eq. (1.c) and t_h the hour (in solar time).

It's important to note that in this study, global radiation is not treated as a singular value but rather as an accumulation over a short period of time (e.g., between h_t and h_{t+1}, using an hourly time step with ERA5-Land). Thus, *sin(β)* needs to be integrated:

https://doi.org/10.5194/egusphere-2024-1800
Preprint. Discussion started: 15 July 2024

$$\int_{h_t}^{h_{t+1}} \sin(\beta) = \sin(\lambda) \times \sin(\delta) + \text{¿¿} \qquad (2)$$

$$\cos(\lambda) \times \cos(\delta) \times \frac{15 \times \pi}{180} \times \left[\sin\left(\frac{\pi}{180} \times 15 \times (h_{t+1} - 12) \right) - \sin\left(\frac{\pi}{180} \times 15 \times (h_t - 12) \right) \right]$$

Then, we used the relationship between the fraction of diffuse radiation (R_{diff}) compared to global radiation data (R_g) and the fraction of global radiation data (R_g) compared to theoretical radiation (R_0), as recommended by de Jon (1980) (described in Spitters et al., 1986):

$$\frac{R_{diff}}{R_g} = 1 \quad \text{for} \quad \frac{R_g}{R_0} \leq 0.22$$

$$\frac{R_{diff}}{R_g} = 1 - 6.4 \times \left(\frac{R_g}{R_0} - 0.22 \right)^2 \quad \text{for} \quad 0.22 < \frac{R_g}{R_0} \leq 0.35 \qquad (3)$$

$$\frac{R_{diff}}{R_g} = 1.47 - 1.66 \times \frac{R_g}{R_0} \quad \text{for} \quad 0.35 < \frac{R_g}{R_0} \leq K$$

$$\frac{R_{diff}}{R_g} = L \quad \text{for} \quad K < \frac{R_g}{R_0}$$

With $L = 0.847 - 1.61 \times \sin(\beta) + 1.04 \times \sin^2(\beta)$ and $K = \frac{1.47 - L}{1.66}$.

Following Spitters et al. (1986), the final step involves subtracting the circumsolar component (R_{circum}) of diffuse radiation from the direct flux.

$$R_{circum} = \cos^2\left(\frac{\pi}{2} - \beta \right) \times \cos^3(\beta) \qquad (4)$$

To determine the corresponding fraction of diffuse radiation under intermediate sky conditions, we adopt the interpolation method introduced by Klucher (1978):

$$\frac{R_{diff}}{R_g} = \frac{R_{diff}}{R_g} \div \left[1 + \left(1 - \left(\frac{R_{diff}}{R_g} \right)^2 \right) \times R_{circum} \right] \qquad (5)$$

Finally, considering that global radiation (R_g) comprises both diffuse (R_{diff}) and direct (R_{dir}) radiation components, the value of R_{dir} can be directly inferred from the other two components.

2.1.2. Downscaling direct radiation

To downscale direct radiation (Fig. 1.ii.), two distinct processes were considered. Firstly, the path of sun rays was examined to determine if any obstruction in the topography may block them. Secondly, if unobstructed, the slope and aspect of the pixel are used to compute the radiation intensity relative to a horizontal surface.

https://doi.org/10.5194/egusphere-2024-1800
Preprint. Discussion started: 15 July 2024

For both processes, the initial step involved computing the sun vector in three dimensions. This was achieved using the R package "insol" (version 1.2.2, Corripio, 2020) and specifically the "sunvector" function, which defines the vector based on longitude, latitude, and time (day, hour, minute). To assess whether radiation is obstructed by a summit, the close topography derived from a DEM is computed using the "doshade" function within the "insol" package. To determine sun intensity, the "hillshading" function from the same package is utilised, requiring both the sun vector and the topography (previously normalised into unit vectors using the "cgrad" function).

Considering that the input radiation is accumulated over a specific period (e.g., 1 hour in ERA5-Land), and to account for spatial variations in radiation intensity (primarily due to the angle of the sun rays) and shadow projections, several time steps are employed for downscaling the direct radiation. In this study, the default value of three time steps per hour (n = 3) was adopted. Additionally, to aggregate the values while considering temporal variations in radiation intensity, each value is weighted by the theoretical extraterrestrial irradiance (R_0 in Eq. (1)). This yields a corrected direct radiation (R_{dir_cor}):

$$R_{dir_{cor}} = R_{dir} \times \frac{\sum_{t_1}^{t_n} \left(R_0 \times S \times \frac{I_{slope}}{I_{vert}} \right)}{\square} \qquad (6)$$

Where S represents the shadow parameter (with a value of 0 indicating shadow and 1 indicating no shadow), and I_{slope} and I_{vert} denote the illumination intensity over the slope and a vertical surface, respectively, to derive the relative intensity of sunlight over the slope.

2.1.3. <u>Downscaling diffuse radiation</u>

Diffuse radiation is independent of the sun's inclination. It emanates uniformly from all directions within the skydome, limited in this study to the top half-sphere. Therefore, its downscaling (Fig. 1.iii) relies on the 360° horizontal surrounding topography, particularly the proportion of diffuse radiation from all directions that can reach the point under study.

Various methods exist to compute this fraction, including employing numerous random rays or determining, for regular 3D distributed vectors, the level of shadow. In this study, a specific method was devised. It involves computing, for each azimuth angle (with fixed steps of 2°), the minimum unshaded radiation using the "doshade" R function described previously and a DEM.

Subsequently, these values are utilised to calculate the shaded area of the top half-sphere and thus the proportion of diffuse radiation reaching the focal point. Finally, this proportion is applied to the diffuse radiation computed in Sect. 2.1.1 to derive the corrected diffuse radiation (R_{diff_cor}).

https://doi.org/10.5194/egusphere-2024-1800
Preprint. Discussion started: 15 July 2024

The corrected diffuse and direct radiation can then be directly employed or recombined into corrected global radiation (R_{g_corr}), e.g., to serve as input to a model of forest function or dynamics.

2.1.4. Digital elevation model data

In various steps of the radiation downscaling, the utilisation of a DEM is imperative (Sect. 2.1.2 and 2.1.3). In this study, we evaluated radiation downscaling using different DEMs characterised by varying resolutions.

The first dataset is the DEM provided by the Shuttle Radar Topography Mission (SRTM, 2013), offering a resolution of 1 arc-second (approximately 30 m). In order to clarify the impact of using different resolutions, the resolution of the SRTM product was downgraded to obtain products with resolutions of 60, 90, 125, 185, 250 and 500 metres using the aggregate function (R, terra 1.7.23 library).

An additional series of DEMs was employed: the Global Multi-resolution Terrain Elevation Data 2010 (GMTED2010, Danielson and Gesch, 2011), which encompasses spatial resolutions of 30, 15, and 7.5 arc-seconds, corresponding approximately to resolutions of 1 km, 500 m, and 250 m, respectively. These datasets were compiled from diverse sources. However, for the metropolitan France region, the primary source of the dataset was the 1 arc-second SRTM DEM.

The interest of these DEMs lies in their applicability beyond the geographic scope covered in this study. Their availability at a global terrestrial scale renders them suitable for use in various locations worldwide (with the exception of SRTM, which is limited to latitudes between 60° north and 56° south).

2.2. Study area

The study area is Mont Ventoux, a mountain located in southeastern France, with its highest point reaching an elevation of 1912 metres (44.174° N - 5.27794° E) (Fig. 2). While Mont Ventoux is predominantly oriented in an east-west direction, it exhibits notable variations in slopes and orientations. The southern flank is characterised by gradual inclines, whereas steeper slopes are evident on its northern side. Mont Ventoux presents a predominantly wooded landscape, featuring a mixed beech-fir forest on its northern side, and a mixed European beech-black pine forest on its southern side, particularly above an elevation of 800 metres (Jean et al., 2023). Below this elevation, the dominant species are more typical of the Mediterranean biome and include coppices of *Quercus pubescens, Quercus ilex, Pinus halepensis* as well as as natural regeneration of *Cedrus atlantica* from old plantation trials of the early 20th century.

https://doi.org/10.5194/egusphere-2024-1800
Preprint. Discussion started: 15 July 2024

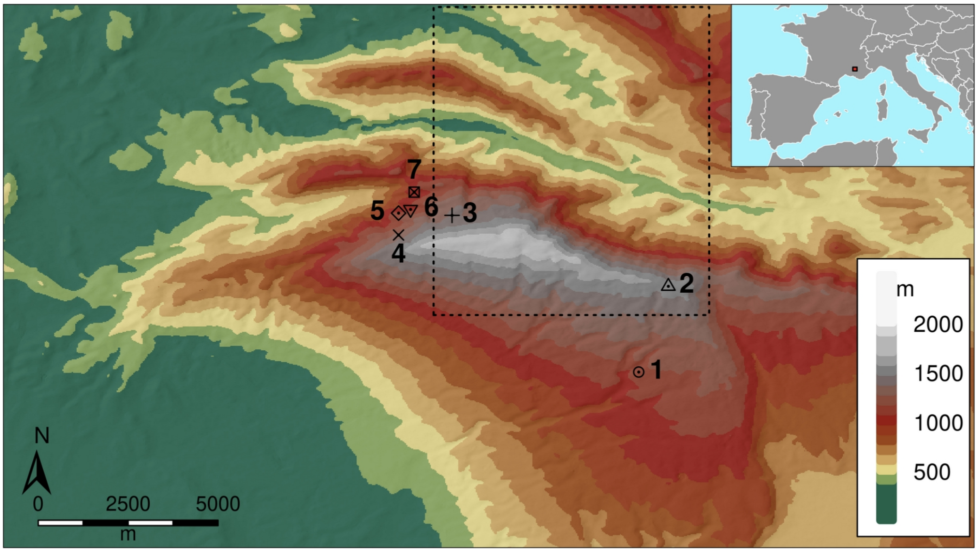

Figure 2: Map of the study area (Mont Ventoux). Mont Ventoux is located in southeastern France (see in the inset). Observation points (one symbol with associated number) and the ERA5-Land tile (in dottle line) used in this study are indicated.

2.3. Radiation measurements

On June, 27 2016, we installed seven mini-weather stations at different strategic elevations and locations on the north face of Mont Ventoux (Table 1), each equipped with loggers (YBdesign) and sensors for photosynthetically active radiation (PAR, 400-700 nm), temperature and relative humidity. The sensors were installed on a vertical pole and positioned horizontally (levelled with a spirit level). The PAR sensors (CBE80, brand Solems) and the thermo-hydrometers (EE07-PFT, brand E+E) were calibrated using a reference weather station at the INRAe campus of Avignon before the beginning of the experiment. The mini-weather stations were positioned in clearings with forest edges extending beyond 30 m from the station. The data were recorded at one hour timestep. The photosynthetic flux density delivered by the sensors were converted into W.m^{-2} of global radiation using an empirical relationship calibrated on the ICOS Font-Blanche experimental site (Moreno et al., 2021).

https://doi.org/10.5194/egusphere-2024-1800
Preprint. Discussion started: 15 July 2024

N°	Site	Latitude (°)	Longitude (°)	Elevation (m)	Slope (°)	Aspect(°)
1	Les Tournières	44.129646	5.320524	1159	5.5	250.1
2	Col de la fache	44.157819	5.331975	1575	6.2	201.2
3	Mont Serein	44.182886	5.257725	1413	4.0	234.1
4	dvx5	44.176758	5.238861	1320	20.8	347.2
5	Tc2	44.184014	5.239161	1116	33.1	351.0
6	dvx2	44.185142	5.243383	1074	28.0	355.1
7	142	44.190856	5.244869	1050	23.0	188.4

Table 1. List and main characteristics of the observation sites in Mont Ventoux where radiation measurements were performed. Slope and aspect was computed from a 30 m resolution SRTM digital elevation model.

The observed radiation is compared with the radiation from ERA5-Land before and after downscaling using DEMs at different resolutions. In order to facilitate the comparison between the ERA5-Land reanalysis dataset and observations, which may contain some gaps due to power failure, we aggregated radiation data over various periods (annually or seasonally). This approach involves excluding time steps with missing data, separately for each site. Moreover, to compare with these observations, the correction of the light intensity due to the angle of the direct light rays in relation to the slope and orientation (Sect. 2.1.2, the 'hillshading' function) was deactivated (in Sect. 3.1), as the measurements were carried out on a device placed horizontally.

2.4. Modelling the effect of radiation downscaling on plant functions

To quantify the influence of downscaled radiation on specific applications, we assessed the impact of radiation downscaling on beech (*Fagus sylvatica*) forest functioning using process-based vegetation modelling on the mountainous area of the Mont Ventoux massif (where radiation measurements were located).

We employed two complementary forest vegetation models to quantify how radiation downscaling affects the spatial patterns of both Gross Primary Productivity (GPP) and drought-induced hydraulic failure. These models are, respectively, the forest growth model CASTANEA (Dufrêne et al., 2005) and the plant hydraulic model SurEau (Cochard et al., 2021; Ruffault et al., 2022).

CASTANEA is a comprehensive forest soil-vegetation-atmosphere model coupled with a growth module. It simulates carbon (photosynthesis and respiration) and water fluxes

https://doi.org/10.5194/egusphere-2024-1800
Preprint. Discussion started: 15 July 2024

(transpiration, soil water content, soil water potential) at a half-hourly to daily time step for an average tree in a homogeneous forest stand. A carbon allocation module assigns a proportion of the daily Net Primary Productivity (NPP) toward various plant compartments (stem, roots, fine roots, flowers, acorn, leaves, and storage) using empirical coefficients. Carbon and water fluxes, including gross and net ecosystem photosynthesis, respiration, transpiration, latent heat fluxes, soil water content, and plant water potential, have been validated on different species and sites, including beech on Mont Ventoux (Davi et al., 2005; Cailleret et al., 2011; Delpierre et al., 2012). In this study, canopy Gross Primary Productivity (GPP) was used to demonstrate the effects of radiation downscaling on potential productivity.

SurEau is a plant-hydraulic model that simulates water fluxes and water potential through various compartments of the soil-plant hydraulic continuum (Cochard et al 2021). At each time step (typically 30 minutes), the model computes leaf stomatal and cuticular transpiration as the product between leaf-to-air vapour pressure deficit (VPD) and stomatal and cuticular conductance. Then, stomatal and cuticular fluxes are used to compute water potential in the different plant compartments, while accounting for the symplasmic capacitance and the hydraulic conductance losses due to xylem embolism. Stomatal closure is regulated in a feedback manner based on leaf water potential through empirical relationships (Klein, 2014; Martin-StPaul et al., 2017). Soil water potential and hydraulic conductance are also computed from soil water content. The model is parameterized with various measurable plant traits previously collected for the target species (Ruffault et al., 2022). In this study, drought-induced embolism (or the percentage loss of hydraulic conductance) in the vascular system was used as a proxy for hydraulic risk during a given summer.

We conducted spatial simulations for one pixel at 0.1° resolution (~ 11 km * 8 km at these coordinates), covering a large part of the Mont Ventoux northern face where the measurements were conducted. The simulations covered the years 2016 and 2017, encompassing the same geographical area as outlined in Sect. 2.3, spanning a segment of Mont Ventoux ranging from 5.25° W to 5.35° W and from 44.15° N to 44.25° N.

Climate data were directly sourced from the ERA5-Land hourly dataset (Muñoz-Sabater et al., 2021), including temperature, precipitation, wind speed, relative humidity, and global radiation. The latter was downscaled using the method presented in Sect. 2.1, employing one of the DEMs discussed in Sect. 2.1.4.
To maintain consistency and avoid introducing uncertainty from disparate datasets, all other non-climatic inputs were set constant across the study area, as described hereafter. The

https://doi.org/10.5194/egusphere-2024-1800
Preprint. Discussion started: 15 July 2024

species selected, *Fagus sylvatica* (European beech), is one of the most common species present on Mont Ventoux (Lander et al., 2021) and its traits are already available for the two models (Cailleret & Davi, 2011; Cailleret et al., 2013 ; Davi & Cailleret, 2017; Ruffault et al., 2022), with a Leaf Area Index set at 3.5. The soil characteristic corresponds to the median value extracted from the whole studied area from the SoilGrids database (Poggio et al., 2021).

3. RESULTS

3.1. Comparison between simulated and observed global radiation

The comparison of ERA5-Land global radiation, both uncorrected and corrected, with observed global radiation across the 7 studied sites shows the benefit of our downscaling method in accurately estimating local global radiation (Fig. 3).

Specifically, the correlation between observed and simulated yearly mean global radiation increases from r^2 = 0.59 to r^2 = 0.93, while the RMSE decreases from 33.5 to 8.6 Wh.m^2, for the raw ERA5-Land radiation and ERA5-Land radiation corrected with a 30 m resolution DEM, respectively (Figs 3a and 3b). However, this increase in the performance of estimating global radiation does not progress consistently as the resolution of our downscaling approach increases. We observe a slight and heterogeneous improvement in the corrected radiation from 1 km to 250 m resolution compared to the raw ERA5-Land resolution (around 9 km). It is not until the resolution reaches around 200 metres that a significant and continuous improvement is observed (decrease in RMSE, increase in r^2) until 30 m resolution (Fig. 3 c).

Our results further show that the absolute performance of radiation models (in terms of r^2) and their relative differences remain consistent across the different studied seasons (Fig. 3a and 3b), despite some particularities. During winter, ERA5-Land raw data shows weak relationship with observations (r^2 at 0.37 and RMSE at 38 Wh.m^2), which substantially improves with correction (r^2 = 0.90, RMSE = 11 Wh.m^2). Similarly, but more pronounced, in autumn correlations and RMSE are considerably enhanced (respectively r^2 from 0.21 to 0.91 and RMSE from 45 to 9 Wh.m^2). In summer, the correlation is almost zero with the ERA5-Land data, whereas it exceeds 0.5 with the corrected radiations. In contrast, the correlation is stable in spring but high (at 0.85), while RMSE is improved with correction (32 to 23 Wh.m^2). Further analysis also reveals that, contrary to Fig. 3 (a), the equations of the seasonal curves for corrected ERA5-Land radiation closely align with the 1/1 line, in accordance with an important decrease in RMSE (Fig. 3 b). It is noteworthy that most of the

https://doi.org/10.5194/egusphere-2024-1800
Preprint. Discussion started: 15 July 2024

improvement comes from points located on northern slopes (points 4, 5 and 6, Fig. 3). Accordingly, the daily bias from those points is reduced compared to uncorrected data, while points located on flat surfaces or southern slopes show similar limited bias (not shown).

https://doi.org/10.5194/egusphere-2024-1800
Preprint. Discussion started: 15 July 2024

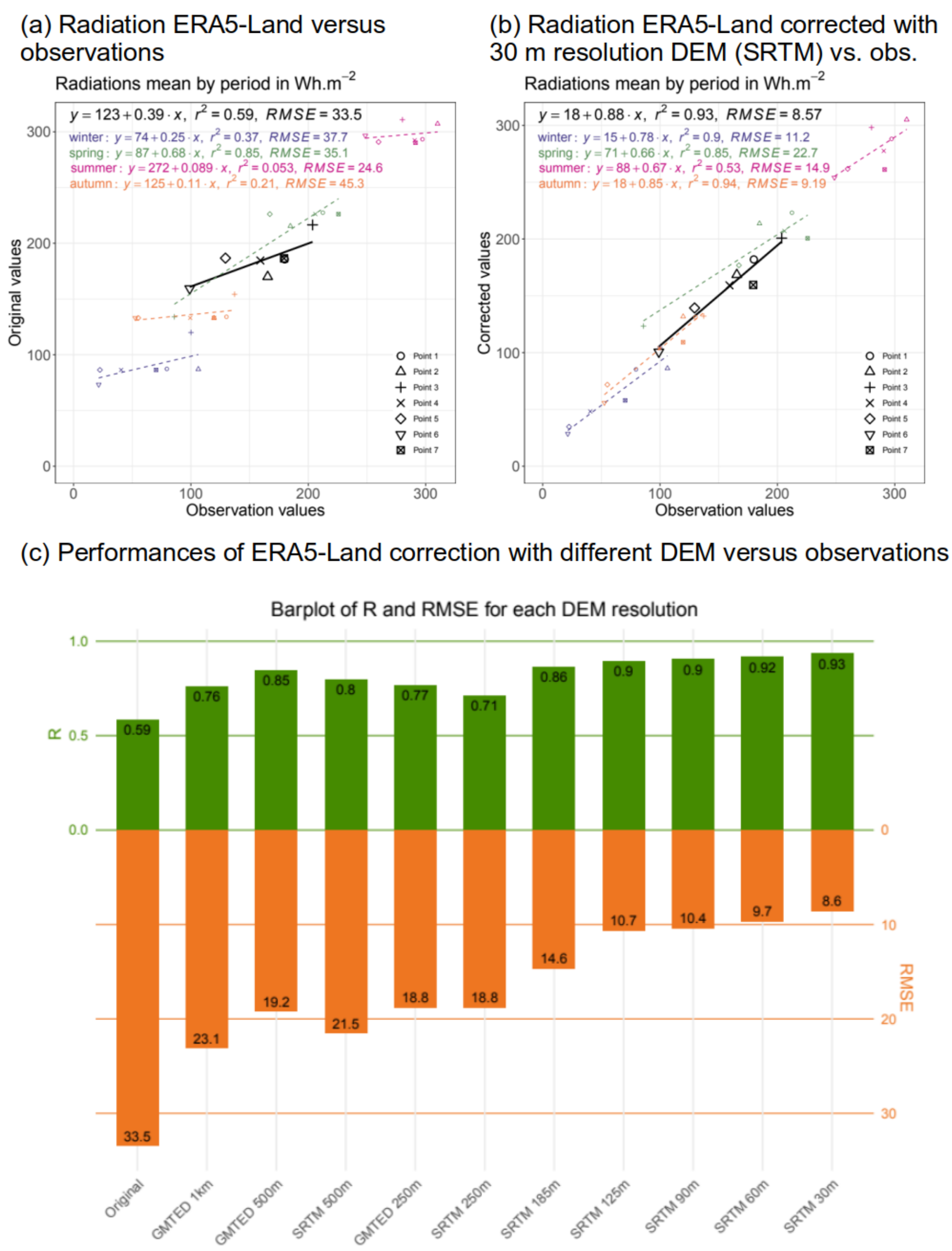

Figure 3: Comparison of the observed radiation with the ERA5-Land product and with corrected radiation from ERA5-Land using different DEMs. (a) and (b) represent the annual and seasonal correlation r² and RMSE (Wh.m²) for each point. (c) shows the annual r² and RMSE (in black in (a) and (b)), for the original ERA5-Land data and each of the corrections obtained with the different DEMs

https://doi.org/10.5194/egusphere-2024-1800
Preprint. Discussion started: 15 July 2024

Figure 4 depicts the global radiation values for two distinct sites during two different periods. Site 1 (refer to Table 1) represents a slightly south-facing location with little shade from topographical features, particularly evident in winter. Site 5, on the other hand, is situated on a north-facing slope (slightly west-facing) affecting sunlight exposure, especially during winter months. Two two-day periods were selected for analysis: one in summer (19 and 20 August 2016) to observe the impact during peak sun exposure and a rainy day (20 August), and another in winter (13 and 14 January 2017) to assess the effect of the downscaling on low-inclination radiation in a mountainous region. Three types of radiation values are presented: observed values (Sect. 2.3), original ERA5-Land values (9 km resolution, tile indicated on Fig. 2), and values following the application of the radiation downscaling with the SRTM DEM (~30 m resolution) (as described in Sect. 2.1, but without “hillshading” function to be comparable with measurement).

At site 1 (Fig. 4.a-b), where surrounding topographical features have minimal impact on radiation, the values from ERA5-Land are close to the observations and there is no significant change after radiation downscaling. These trends hold for both clear and cloudy days, and for both winter and summer periods. At site 5, disparities between original and corrected ERA5-Land values are more significant due to topographical influences. In summer (Fig. 4.c), discrepancies exist between original and corrected ERA5-Land values. Corrected values more closely represent measured values but still struggle to replicate sub-daily variations. Particularly, a dip in the curve around 10am appears to be present on both days, possibly indicating a shadow, but not represented in the corrected radiation. In winter (Fig. 4.d), downscaling markedly impacts radiation values, with corrected values nearly four times lower than ERA5-Land values, closely aligning with observed values.

Note that if the effect of the slope and orientation were activated, the effect of the light intensity would be to potentially increase the corrected radiation on the south faces, mainly on clear days and in winter (e.g. +10 % for point 1), and on the contrary to considerably reduce the corrected radiation on cloud-free day (e.g. by two for 19 August at point 5).

https://doi.org/10.5194/egusphere-2024-1800
Preprint. Discussion started: 15 July 2024

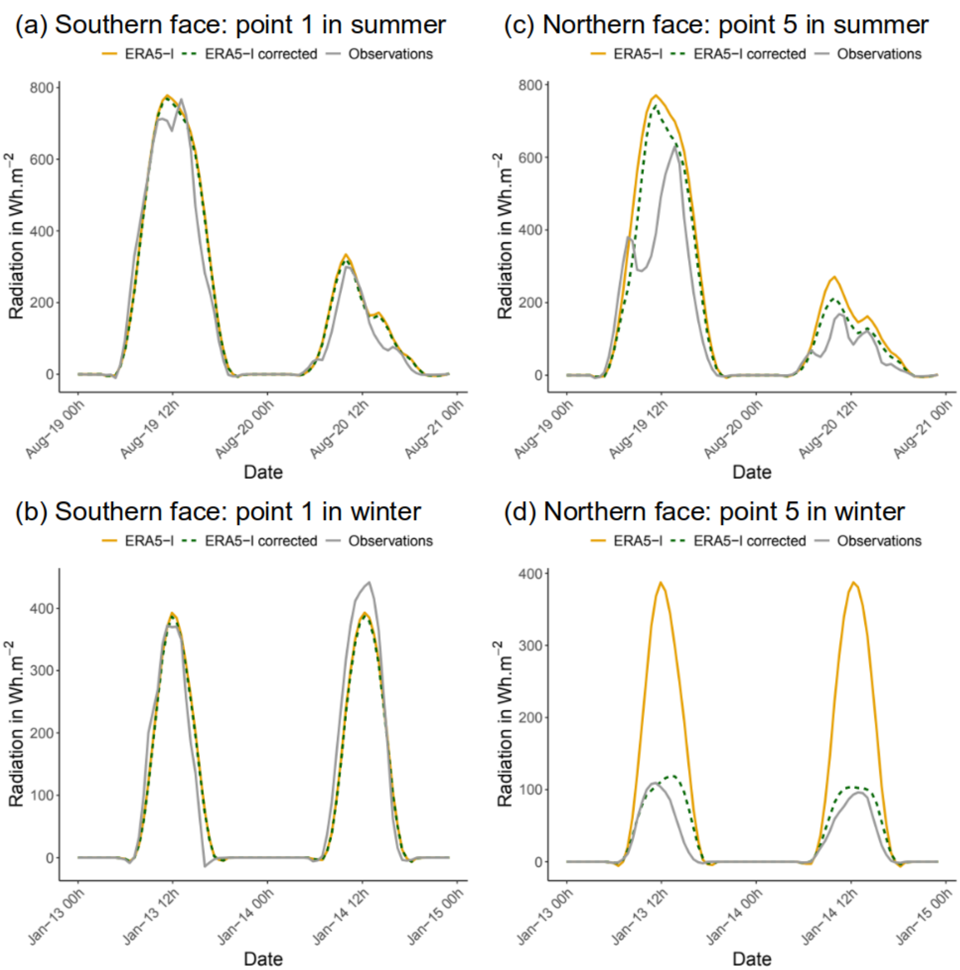

Figure 4: Radiation of original ERA5-Land data in orange, after downscaling with the SRTM DEM (30 m resolution) in dotted dark green and the observations in grey, for site 1 (a and b) and site 5 (c and d) and for two different dates: one in summer (19-20 August 2016 in a and c) and one in winter (13-14 January 2017 in b and d)

3.2. Application on Mont Ventoux massif

3.2.1. Heterogeneity of global radiation

Applying our approach across a heterogeneous geographical area illustrates the spatial and temporal variability in global radiation introduced by downscaling (Fig. 5).

Radiation downscaling exerts a clear impact in the mountainous region under study, halving original ERA5-Land global radiation. An evident differentiation emerges between south-facing slopes, which receive more radiation, and north-facing slopes, which exhibit minimal radiation levels in winter (approaching zero). Mean radiation values decrease with increasing

https://doi.org/10.5194/egusphere-2024-1800
Preprint. Discussion started: 15 July 2024

resolution of the three DEM used, indicating an average decrease of 10.7 % on 13 January 2017 and 5.9 % on 19 August 2016 when transitioning from the GMTED DEM at approximately 500 metres to the SRTM at approximately 30 metres resolution. Conversely, standard deviation increases with resolution, rising by 13.5 % and 30.0 %, respectively. However, during winter, the standard deviation mirrors the magnitude of the mean due to low radiation values, whereas in summer, it accounts for 20 to 25 % of the mean.

These differences in standard deviation due to topography imply significant differences between the different DEMs, as well as with the original ERA5-Land values. For instance, the maximum radiation value recorded on January 13th totals 7.3 $MJ.m^{-2}$ in the reanalysis, whereas it reaches 9.3 $MJ.m^{-2}$ with downscaling conducted using the 250 m DEM. Similarly, on January 13th (Fig. 5.b), the spatial pattern representing a denser "line" denoting stronger radiation values around 5.3° E and 44.19° N is relatively narrow with the 30 m DEM (approximately 200 meters wide), whereas it doubles in width with the 500 m DEM.

https://doi.org/10.5194/egusphere-2024-1800
Preprint. Discussion started: 15 July 2024

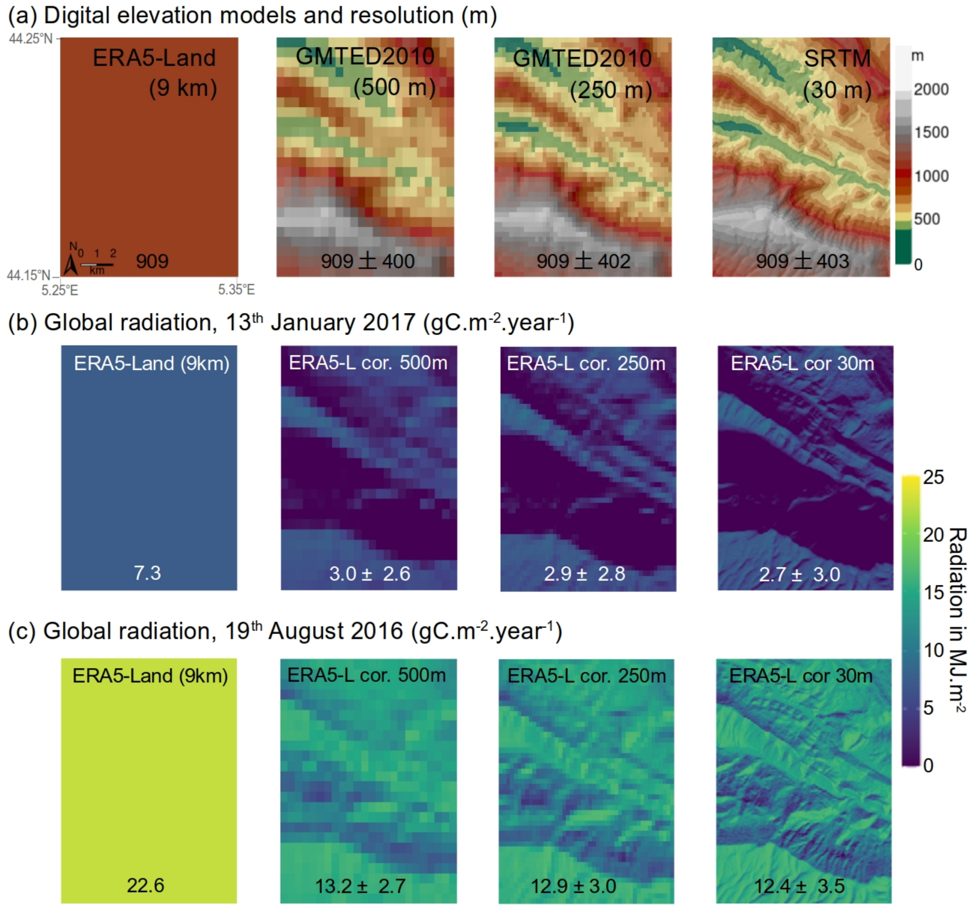

Figure 5: Global radiation from ERA5-Land and resulting from downscaling obtained from different resolution DEMs. (a) ERA5-Land tile (left) and DEM resolution (500, 250, and 30 metres, from left to right). Global radiation for two distinct dates, (b) in winter (13 January 2017) and (c) in summer (19 August 2016). Regional mean values and standard deviations are indicated on the bottom of each map.

3.2.2. Modelling the influence of radiation downscaling on vegetation functioning

Modifying radiation across the entire area according to each DEM has a tangible impact as presented on models output as shown in Fig. 6. In general, the simulations remain consistent across the studied area, despite potential variations introduced by the different topographies used during downscaling. With downscaling, there is a discernible reduction in Gross Primary Productivity (GPP) ranging between 5 % and 8 %, as well as in the risk of

https://doi.org/10.5194/egusphere-2024-1800
Preprint. Discussion started: 15 July 2024

hydraulic failure, which decreases between 14 % and 23 %. Moreover, the standard deviation introduced between the values is quite significant, varying between 8 % and 13 % for the two outputs studied.

Upon comparing the patterns obtained with the corresponding DEMs, it becomes evident that south-facing slopes tend to exhibit higher annual productivity (Fig. 6.b) but are susceptible to greater hydraulic stress (as indicated by darker colours in Fig. 6.c). Conversely, north-facing slopes generally manifest lower GPP as simulated by the Castanea model, yet exhibit a reduced risk of hydraulic failure.

To evaluate the potential impact of these discrepancies on mortality risk, we computed the risk of hydraulic failure from the embolism simulations. The relationship between mortality and embolism level water stress is often conceptualised as a threshold effect (Choat et al., 2018), although this notion is occasionally questioned (Hammond et al., 2021). Setting the threshold at which mortality occurs to 50 % of risk of hydraulic failure, we obtain mortality percentages in term of surface of 100 %, and 97 %, 98 % and 89 % for the original ERA5-Land tile, and the data downscaled to 500 m, 250 m and 30 m, respectively. Given that the useful reserve used in this study comes from a single value taken from the median over the area of the SoilGrids database (Poggio et al., 2021), and that this value is open to question, these results must be compared relatively to each other.

https://doi.org/10.5194/egusphere-2024-1800
Preprint. Discussion started: 15 July 2024

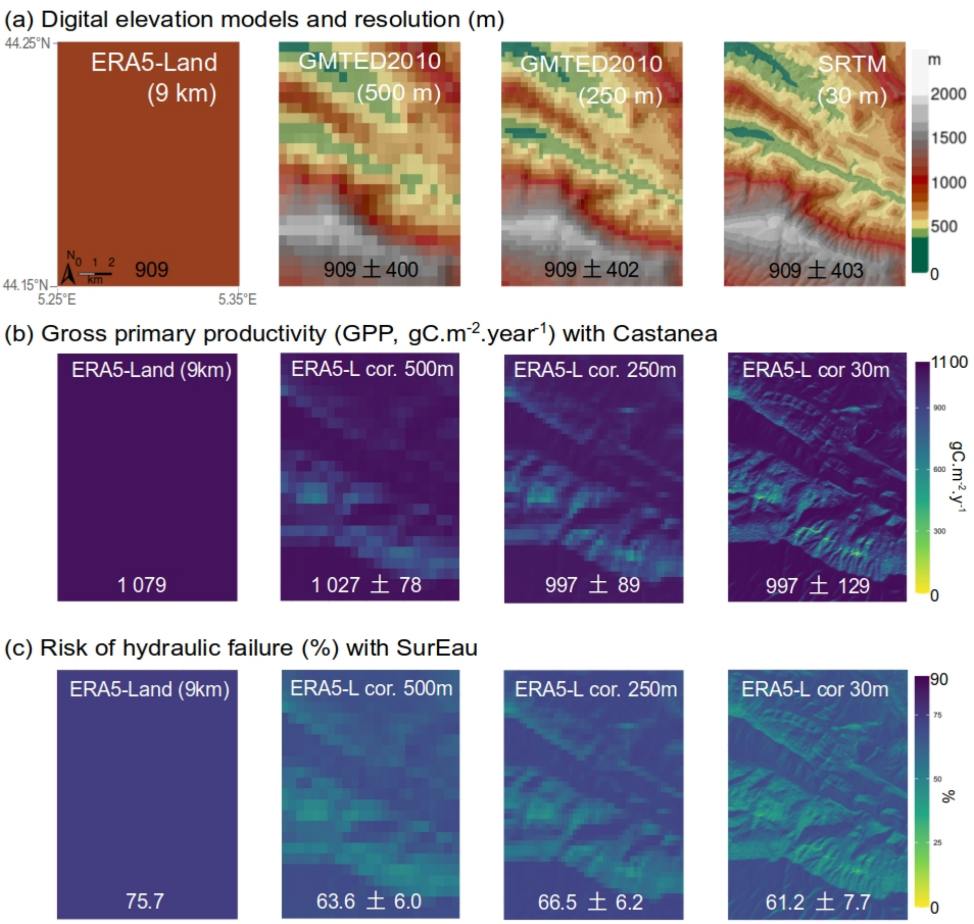

Figure 6: Gross primary productivity and risk of hydraulic failure simulated with, respectively, Castanea and SurEau, from ERA5-Land and resulting from global radiation downscaling obtained from different resolution DEMs. (a) ERA5-Land tile (left) and DEM resolution (500, 250, and 30 metres, from left to right). (b) Gross primary productivity simulated with Castanea. (c) Risk of hydraulic failure simulated with SurEau. Regional mean values and standard deviations are indicated on the bottom of each map.

4. DISCUSSION

4.1. Performance of the downscaling method

The results of our study indicate that the radiation downscaling method developed in this study effectively captures the overall trend of radiation distribution across mountainous regions. The daily patterns are effectively represented, however sub-daily variations may not fully account for microclimatic variations, especially considering the spatial heterogeneity within a grid pixel at the resolution of climate data. This is the case for example with cloud cover, which can be highly variable in mountainous regions.

However, our findings suggest that, overall, radiation downscaling significantly reduces radiation levels on the north-facing side, particularly during winter, as a result of the obstruction of direct radiation by surrounding mountains. Conversely, this radiation decrease on north-facing slopes is compensated by an increase on south-facing slopes. Consequently our method improves methods already available to downscale radiation (Piedallu & Gégout, 2008).

The results of our radiation downscaling method reveal a significant improvement of the representation of radiation from 9 km reanalysis, for all seasons, but especially on north-facing slopes and more pronounced in winter. The impact of radiation downscaling is therefore primarily observed in regions with significant shadow casting, and it becomes more pronounced with the sun's zenithal angle. This emphasises the necessity to correct the radiation to accurately depict the dynamics of radiation in mountainous regions. Nevertheless, the method has its limitations, as it is linked to the quality of DEM and does not take into account climatic heterogeneity, which can explain cloud cover on a smaller scale than the reanalysis data. Thus in Figure 4.c, the dip at around 10am may indicate the presence of micro-climatic conditions, such as fog, an effect that was not considered in our downscaling method.

Additionally, our analysis revealed intriguing results concerning the impact of different DEM resolutions. While no clear improvement was observed with a resolution greater than 250 m, a clear gradual improvement appears for resolutions finer than 250 m (up to 30 m). This suggests that higher resolutions are crucial for effectively capturing the nuances of radiation dynamics. We hypothesise that insufficient improvement in resolution during the downscaling introduces some variance which is not adequately compensated by improvements in radiation representation at the site level.

4.2. Implications of downscaling for modelling studies

The application of downscaling with the SurEau and CASTANEA models provides an overview of the impact that downscaling can have on different parameters, such as GPP or tree mortality risk due to hydraulic failure. Mont Ventoux was used as a benchmark site for testing applications. The impact of downscaling on these parameters is most pronounced in

https://doi.org/10.5194/egusphere-2024-1800
Preprint. Discussion started: 15 July 2024

areas with significant topographic features, such as mountainous regions or canyons, with lower radiation levels on north-facing slopes due to shading and higher radiation levels on south-facing slopes due to sun intensity.

These findings have to be taken with caution as only radiation was downscaled making the other forcing variables (temperature, VPD, rainfall) decorrelated which partly limits the interpretation. However, with these limits in my mind and assuming impact models can be used to assess climate products in this context (Stephanon et al., 2015), it appears that radiation downscaling has profound implications on impact simulation (Fig. 6). In particular when considering processes that are based on threshold, such as the mortality risk associated with hydraulic failure, in our example, the mortality rate can go from 100 % to 89 %. Thus, assessing the spatial heterogeneity of radiation, through its interaction with topography, seems crucial for accurately assessing ecological responses and potential threshold effects in complex terrain. Future studies could benefit from these methods to improve the prediction of species distribution or ecosystem functions at local level.

5. CONCLUSION

In this study, we developed a process-based method to downscale global radiation data made on flat surfaces, such as coarse spatial resolution global reanalysis data. The method builds upon existing research and goes further than traditional process-based radiation downscaling methods, by accounting for the shadowing effect on direct radiation and for the bowl effect on diffuse radiation (Piedallu & Gégout, 2008). The recent ERA5-Land hourly data available at 9 km resolution was used to compare on the Mont Ventoux the impact of radiation downscaling computed from different digital elevation models.

The radiation downscaling method effectively captures the overall trend of radiation distribution across mountainous regions. Downscaled radiation is improved compared to original ERA5-Land data, especially during winter months, due to the higher zenithal angle. However, the improvement is significant only after a certain spatial resolution (~ 150 m) and gradually increases thereafter. The implications of downscaling for modelling studies was further investigated using two different process-based models representing gross primary productivity and risk of hydraulic failure. The impact of downscaling on those is most pronounced in areas with significant topographic features, such as mountainous regions or canyons. Assessing the spatial heterogeneity of radiation, through its interaction with topography, is crucial for accurately addressing ecological responses and potential threshold effects in complex terrain.

The method can be applied at any resolution, depending on the choice of the DEM. Moreover, it relies on any type of radiation data, making it applicable to any region in the world and to historical periods as well as future projections. Finally, the method could involve other types of climatic data from the same input dataset, such as temperature or precipitation, thereby ensuring physical consistency between the variables. In the future such methods could be included in more generic climate downscaling tools (e.g. Meteoland, De Cáceres et al., 2018) to facilitate the application of process based models at fine resolution.

Code availability

The scripts corresponding to the method developed in this article is available on GitLab at https://forgemia.inra.fr/urfm/modeldata_toolkit (commit afc05ed2) with the prefix “RadDownscaling”.

The SurEau model code presented in section 2.4 and whose results are presented in section 3.2 is available on GitLab at https://forgemia.inra.fr/urfm/sureau (commit ca19abfb), while the CASTANEA version is available on the capsis platform (https://capsis.cirad.fr/, lasted access the 12/06/2024) and can be downloaded from the "download" menu.

Data availability

Data from Mont Ventoux (2016-2017) at the seven sites are provided by URFM-INRAE Avignon. The full dataset and site information can be accessed from https://doi.org/10.57745/B22AUG.

DEM data are freely accessible and can be downloaded from https://earthexplorer.usgs.gov/ (last accessed 12/06/2024): the Global Multi-resolution Terrain Elevation Data 2010 (GMTED2010) (https://doi.org/10.5066/F7J38R2N) and the Shuttle Radar Topography Mission (SRTM) 1 Arc-Second Global (https://doi.org/10.5066/F7PR7TFT).

Climate ERA5-Land data (https://doi.org/10.24381/cds.e2161bac), including global radiation, are provided by Copernicus and can be directly downloaded from https://cds.climate.copernicus.eu/cdsapp#!/dataset/reanalysis-era5-land?tab=form (last accessed 12/06/2024).

Author contribution

Druel, A., Ruffault, J., Davi, H. and Martin-StPaul, N.K. designed the research and performed the research. Druel, A. developed the scripts and the figures. Marloie, O. and Martin-StPaul, N.K. collected the data on Mont Ventoux. Druel, A., Ruffault, J., Davi, H., De Cáceres, M., Mouillot, F., François, C. and Martin-StPaul, N.K. interpreted the results. Druel,

A. led the writing of the manuscript with inputs from Ruffault, J., Chanzy, A., Marloie, O., De Cáceres, M., Mouillot, F., François, C., Soudani, K., and Martin-StPaul, N.K.

Competing interests

The authors declare that they have no conflict of interest.

Acknowledgements

This project received funding from the European Union's Horizon 2020 research and innovation program under Grant Agreement No. 862221 (FORGENIUS). The authors would also like to thank William Brunetto (URFM, INRAE, Avignon, France) for his help with data acquisition on Mont Ventoux and Deborah Verfaillie for her help with proofreading.

https://doi.org/10.5194/egusphere-2024-1800
Preprint. Discussion started: 15 July 2024

References

Austin, M.P., Nicholls, A.O. and Margules, C.R.: Measurement of the realised qualitative niche: Environmental niches of five Eucalyptus species. *Ecological Monographs*, 60(2): 161-177, https://doi.org/10.2307/1943043, 1990.

Bailey, M. D., Nychka, D., Sengupta, M., Habte, A., Xie, Y., and Bandyopadhyay, S.: Regridding uncertainty for statistical downscaling of solar radiation. *Adv. Stat. Clim. Meteorol. Oceanogr.*, 9, 103–120, https://doi.org/10.5194/ascmo-9-103-2023, 2023

Bedia, J., Herrera, S. and Gutiérrez, J.M.: Dangers of Using Global Bioclimatic Datasets for Ecological Niche Modeling. Limitations for Future Climate Projections. *Global and Planetary Change*, 107, 1-12, http://dx.doi.org/10.1016/j.gloplacha.2013.04.005, 2013.

Bird, R. E., and Hulstrom, R. L.: A simplified clear sky model for direct and diffuse insolation on horizontal surfaces. *Solar Energy Research Institute*, TR-642-761, 1981.

Bramer, I., Anderson, B.J., Bennie, J., Bladon, A.J., De Frenne, P., Hemming, D., Hill, R.A., Kearney, M.R., Körner, C.,Korstjens, A.H., Lenoir, J., Maclean, I.M.D., Marsh, C.D., Morecroft, M.D., Ohlemüller, R., Slater, H.D., Suggitt, A.J., Zellweger, F. and Gillingham, P.K.: Advances in monitoring and modelling climate at ecologically relevant scales. *Advances in Ecological Research*, 58, 101–161.https://doi.org/10.1016/bs.aecr.2017.12.005, 2018.

Brun, P., Zimmermann, N. E., Hari, C., Pellissier, L. and Karger, D. N.: CHELSA-BIOCLIM+ A novel set of global climate-related predictors at kilometre-resolution. *EnviDat.*, https://www.doi.org/10.16904/envidat.332, 2022.

Cailleret, M. and Davi, H.: Effects of climate on diameter growth of co-occurring *Fagus sylvatica* and *Abies alba* along an altitudinal gradient. *Trees*, 25:265–276. https://doi.org/10.1007/s00468-010-0503-0, 2011.

Cailleret M., Nourtier M., Amm A., Durand-Gillmann M. and Davi H.: Drought-induced decline and mortality of silver fir differ among three sites in Southern France. *Annals of Forest Science*, 71, 643–657, 2013.

Carroll, C., Zielinski, W.J. and Noss, R.F.: Using presence-absence data to build and test spatial habitat models for the Fisher in the Klamath region, U.S.A. *Conservation Biology*, 13(6): 1344-1359, https://doi.org/10.1046/j.1523-1739.1999.98364.x, 1999.

Clark, D.B., Palmer, M.W. and Clark, D.A.: Edaphic factors and the landscape-scale distributions of tropical rain forest trees. *Ecology*, 80(8): 2662-2675, https://doi.org/10.1890/0012-9658(1999)080[2662:EFATLS]2.0.CO;2, 1999.

Choat, B., Brodribb, T. J., Brodersen, C. R., Duursma, R. A., López, R. and Medlyn, B. E.: Triggers of tree mortality under drought. *Nature*, 558(7711), 531–539. https://doi.org/10.1038/s41586-018-0240-x, 2018.

Churkina, G., and Running, S. W.: Contrasting Climatic Controls on the Estimated

https://doi.org/10.5194/egusphere-2024-1800
Preprint. Discussion started: 15 July 2024

Productivity of Global Terrestrial Biomes. *Ecosystems*, 1(2), 206–215. https://doi.org/10.1007/s100219900016, 1998.

Cochard, H., Pimont, F., Ruffault, J. & Martin-StPaul, N.: SurEau: a mechanistic model of plant water relations under extreme drought. *Ann. For. Sci.*, 78, https://doi.org/10.1007/s13595-021-01067-y, 2021.

Danielson, J.J., and Gesch, D.B.: Global multi-resolution terrain elevation data 2010 (GMTED2010): U.S. Geological Survey Open-File Report 2011–1073, 26 p., https://doi.org/10.5066/F7J38R2N (Downloaded on https://earthexplorer.usgs.gov/ the 15-10-2021), 2011.

Davi, H., Dufrêne, E., Granier, A., Le Dantec, V., Barbaroux, C., François, C. and Bréda, N. Modelling carbon and water cycles in a beech forest: Part II.: Validation of the main processes from organ to stand scale. *Ecological Modelling*, 185, 387–405. doi:10.1016/j.ecolmodel.2005.01.003, 2005.

Davi, H., Dufrêne, E., Francois, C., Le Maire, G., Loustau, D., Bosc, A., Rambal, S., Granier A. and Moors E.: Sensitivity of water and carbon fluxes to climate changes from 1960 to 2100 in European forest ecosystems. *Agric. For. Meteorol.*, 141, 35–56, https://doi.org/10.1016/j.agrformet.2006.09.003, 2006.

Davi, H. and Cailleret, M.: Assessing drought-driven mortality trees with physiological process-based models. *Agricultural and Forest Meteorology*, 232, 279–290, https://doi.org/10.1016/j.agrformet.2016.08.019, 2017.

Davy, R. and Kusch, E.: Reconciling high resolution climate datasets using KrigR. *Environ. Res. Lett.*, 16, 124040, https://doi.org/10.1088/1748-9326/ac39bf, 2021.

De Cáceres, M., Martínez-Vilalta, J., Coll, L., Llorens, P., Casals, P., Poyatos, R., Pausas, J.G. and Brotons, L.: Coupling a water balance model with forest inventory data to predict drought stress: the role of forest structural changes vs. climate changes. *Agricultural and Forest Meteorology*, 213: 77-90, https://doi.org/10.1016/j.agrformet.2015.06.012, 2015.

De Cáceres, M., Martin-StPaul, N., Turco, M., Cabon, A. and Granda, V.: Estimating daily meteorological data and downscaling climate models over landscapes. *Environmental Modelling and Software*, 108: 186-196, doi:10.1016/j.envsoft.2018.08.003, 2018.

De Cáceres M, Molowny-Horas R, Cabon A, Martínez-Vilalta J, Mencuccini M, García-Valdés, R., Nadal-Sala, D., Sabaté, S., Martin-StPaul, N., Morin, X., D'Adamo, F., Batllori, E. and Améztegui, A.: MEDFATE 2.9.3: A trait-enabled model to simulate Mediterranean forest function and dynamics at regional scales. *Geoscientific Model Development*, 16, 3165–3201, https://doi.org/10.5194/gmd-16-3165-2023, 2023.

De Jong, J.B.R.M.: Een karakterisering van de zonnestraling (A characterization of solar radiation) in Nederland. Doctoral report, Eindhoven University of Technology, Netherlands, 97 + 67 pp., 1980.

https://doi.org/10.5194/egusphere-2024-1800
Preprint. Discussion started: 15 July 2024

Delpierre, N., Soudani, K., Franc¸ ois, C., Le Maire, G., Bernhofer, C., Kutsch, W., Misson, L., Rambal, S., Vesala, T., and Dufrêne, E.: Quantifying the influence of climate and biological drivers on the interannual variability of carbon exchanges in European forests through process-based modelling. *Agric. For. Meteorol.*, 154–155, 99–112, https://doi.org/10.1016/j.agrformet.2011.10.010, 2012.

Dirnbock, T., Dullinger, S., Gottfried, M., Ginzler, C. and Grabherr, G.: Mapping alpine vegetation based on image analysis, topographic variables and Canonical Correspondance Analysis. *Applied Vegetation Science*, 6: 85-96, https://doi.org/10.1111/j.1654-109X.2003.tb00567.x, 2003.

Dubayah, R. and Loechel, S.: Modeling topographic solar radiation using GOES data. J. *Appl. Meteor.*, 36, 141–154, https://doi.org/10.1175/1520-0450(1997)036<0141:MTSRUG>2.0.CO;2, 1997.

Dufrêne, E., Davi, H., François, C., Maire, G. l., Dantec, V. L., and Granier, A.: Modelling carbon and water cycles in a beech forest: Part I: Model description and uncertainty analysis on modelled NEE. *Ecol. Model.*, 185, 407–436, https://doi.org/10.1016/j.ecolmodel.2005.01.004, 2005.

Fealy, R. and Sweeney, J.: Statistical downscaling of temperature, radiation and potential evapotranspiration to produce a multiple GCM ensemble mean for a selection of sites in Ireland. *Irish Geography*, 41:1, 1-27, DOI: https://doi.org/10.1080/00750770801909235, 2008.

Fisher, J. B., Whittaker, R. J., and Malhi, Y.: ET come home: Potential evapotranspiration in geographical ecology: ET come home. *Global Ecology and Biogeography*, 20(1), 1–18. https://doi.org/10.1111/j.1466-8238.2010.00578.x, 2011.

Franklin, J.: Predicting the distribution of shrub species in southern California from climate and terrain-derived variables. *Journal of Vegetation Science*, 9(5): 733-748, https://doi.org/10.2307/3237291, 1998.

Corripio, J.G.: insol: Solar Radiation. R package version 1.2.2, https://www.meteoexploration.com/R/insol/ (last access 27/05/2024), 2020.

Granier, A., Breda, N., Biron, P. and Villette, S.: A lumped water balance model to evaluate duration and intensity of drought constraints in forest stands. *Ecol. Model.*, 116:269–283, https://doi.org/10.1016/S0304-3800(98)00205-1, 1999.

Granier, A., Reichstein, M., Bréda, N., Janssens, I. A., Falge, E., Ciais, P., Grünwald, T., Aubinet, M., Berbigier, P., Bernhofer, C., Buchmann, N., Facini, O., Grassi, G., Heinesch, B., Ilvesniemi, H., Keronen, P., Knohl, A., Köstner, B., Lagergren, F., Lindroth, A., Longdoz, B., Loustau, D., Mateus, J., Montagnani, L., Nys, C., Moors, E.J., Papale, D., Peiffer, M., Pilegaard, K., Pita, G., Pumpanen, J., Rambal, S., Rebmann, C., Rodrigues, A., Seufert, G., Tenhunen, J., Vesala, T. and Wang, Q.: Evidence for soil water control on carbon and water

https://doi.org/10.5194/egusphere-2024-1800
Preprint. Discussion started: 15 July 2024

dynamics in European forests during the extremely dry year: 2003. *Agricultural and Forest Meteorology*, 143(1-2), 123-145. https://doi.org/10.1016/j.agrformet.2006.12.004, 2007.

Hammond, W. M., Yu, K., Wilson, L. A., Will, R. E., Anderegg, W. R. L. and Adams, H. D.: Dead or dying? Quantifying the point of no return from hydraulic failure in drought-induced tree mortality. *New Phytologist*, 223(4), 1834–1843, https://doi.org/10.1111/nph.15922, 2019.

Hernanz, A., Correa, C., Domínguez, M., Rodríguez-Guisado, E. and Rodríguez-Camino, E.: Comparison of machine learning statistical downscaling and regional climate models for temperature, precipitation, wind speed, humidity and radiation over Europe under present conditions. *International Journal of Climatology*, 43, 13, 6065-6082, https://doi.org/10.1002/joc.8190, 2023.

Hijmans, R.J., Cameron, S.E., Parra, J.L., Jones, P.G. and Jarvis, A.: Very high-resolution interpolated climate surfaces for global land areas. *International Journal of Climatology*, 25(15):1965-1978, https://doi.org/10.1002/joc.1276, 2005.

I.E.A. (International Energy Agency): An Introduction to Meteorological Measurements and Data. Handling for Solar Energy Applications, Handbook Int. Energy Agency, Dept. Energy U.S.A., Washington D.C, 1978.

Jean, F., Davi, H., Oddou-Muratorio, S., Fady, B., Scotti, I., Scotti-Saintagne, C., Ruffault, J., Journe, V., Clastre, P., Marloie, O., Brunetto, W., Correard, M., Gilg, O., Pringarve, M., Rei, F., Thevenet, J., Turion, N. and Pichot, C.: A 14-year series of leaf phenological data collected for European beech (*Fagus sylvatica L.*) and silver fir (*Abies alba Mill.*) from their geographic range margins in south-eastern France. *Annals of Forest Science*, (2023)80:35, https://doi.org/10.1186/s13595-023-01193-9, 2023.

Klein, T.: The variability of stomatal sensitivity to leaf water potential across tree species indicates a continuum between isohydric and anisohydric behaviours. *Funct. Ecol.*, 28, 1313–1320, https://doi.org/10.1111/1365-2435.12289, 2014.

Klucher, T.M.: Evaluation of models to predict insolation on tilted surfaces. Division of *solar energy,* N.A.S.A. TM-78842, https://doi.org/10.1016/0038-092X(79)90110-5, 1978.

Lander, T.A., Klein, E.K., Roig, A. and Oddou-Muratorio, S.: Weak founder effects but significant spatial genetic imprint of recent contraction and expansion of European beech populations. *Heredity (Edinb)*, 126(3):491-504, doi: 10.1038/s41437-020-00387-5, 2021.

Martin-StPaul, N., Delzon, S. and Cochard, H.: Plant resistance to drought depends on timely stomatal closure. *Ecology Letters*, 20(11), 1437–1447. https://doi.org/10.1111/ele.1285, 2017.

Martin-StPaul, N., Ruffault, J., Guillemot, J., Barbero, R., Cochard, H., Cailleret, M., Cáceres, M. D., Dupuy, J.-L., Pimont, F., Torres-Ruiz, J. M., and Limousin, J.-M.: How much does VPD drive tree water stress and forest disturbances? *Authorea,* Preprints.

https://doi.org/10.5194/egusphere-2024-1800
Preprint. Discussion started: 15 July 2024

https://doi.org/10.22541/au.168147010.01270793/v1, 2023.

Meentemeyer, R.K., Moody, A. and Franklin, J.: Landscape-scale patterns of shrub-species abundance in California chaparral: The role of topographically mediated resource gradients. *Plant Ecology*, 156: 19-41, https://doi.org/10.1023/A:1011944805738, 2001.

Monteith, J. L.: Evaporation and surface temperature. *Quarterly Journal of the Royal Meteorological Society*, 107(451), 1–27. https://doi.org/10.1002/qj.49710745102, 1981.

Moreno, M., Simioni, G., Cailleret, M., Ruffault, J., Badel, E., Carrière, S., Davi, H., Gavinet, J., Huc, R., Limousin, J.-M., Marloie, O., Martin, L., Rodríguez-Calcerrada, J., Vennetier, M. and Martin-StPaul, N.: Consistently lower sap velocity and growth over nine years of rainfall exclusion in a Mediterranean mixed pine-oak forest. *Agricultural and Forest Meteorology*, 308–309, 108472. https://doi.org/10.1016/j.agrformet.2021.108472, 2021.

Muñoz-Sabater, J., Dutra, E., Agustí-Panareda, A., Albergel, C., Arduini, G., Balsamo, G., Boussetta, S., Choulga, M., Harrigan, S., Hersbach, H., Martens, B., Miralles, D. G., Piles, M., Rodríguez-Fernández, N. J., Zsoter, E., Buontempo, C., and Thépaut, J.-N.: ERA5-Land: a state-of-the-art global reanalysis dataset for land applications. *Earth Syst. Sci. Data*, 13, 4349–4383, https://doi.org/10.5194/essd-13-4349-2021, 2021.

Oliphant, A. J., & Stoy, P. C.: An evaluation of semiempirical models for partitioning photosynthetically active radiation into diffuse and direct beam components. Journal of GeophysicalResearch: *Biogeosciences*, 123, 889–901, https://doi.org/10.1002/2017JG004370, 2018.

Patsiou, T.S., Conti, E., Zimmermann, N.E., Theodoridis, S. and Randin, C.F.: Topo-climatic microrefugia explain the persistence of a rare endemic plant in the Alps during the last 21 millennia. *Global Change Biology*, 20(7):2286–2300, https://doi.org/10.1111/gcb.12515, 2014.

Piedallu, C. and Gégout, J.-C.: Multiscale computation of solar radiation for predictive vegetation modelling. *Ann. For. Sci.*, 64, 899-909, DOI: 10.1051/forest:2007072, 2007.

Piedallu, C. and Gégout, J-C.: Efficient assessment of topographic solar radiation to improve plant distribution models. *Agricultural and Forest Meteorology*, 148 (11), pp.1696-1706., https://doi.org/10.1016/j.agrformet.2008.06.001, 2008.

Pierce, K.B., Lookingbill, T. and Urban, D.: A simple method for estimating potential relative radiation (PRR) for landscape-scale vegetation analysis. *Landscape Ecology*, 20(2): 137-147, https://doi.org/10.1007/s10980-004-1296-6, 2005.

Poggio, L., De Sousa, L. M., Batjes, N. H., Heuvelink, G. B. M., Kempen, B., Ribeiro, E., and Rossiter, D.: SoilGrids 2.0: Producing soil information for the globe with quantified spatial uncertainty. *Soil*, 7(1), 217–240. doi: 10.5194/soil-7-217-2021, 2021.

Randin, C. F., Engler, R., Normand, S., Zappa, M., Zimmermann, N. E., Pearman, P. B., Vittoz, P., Thuiller, W. and Guisan, A.: Climate change and plant distribution: local models predict high-elevation persistence. *Global Change Biology*, 15(6), 1557-1569. https://doi.org/10.1111/j.1365-2486.2008.01766.x, 2009.

Roderick, M. L.: Estimating the diffuse component from daily and monthly measurements of global radiation. *Agricultural and Forest Meteorology*, 95, 169-185, https://doi.org/10.1016/S0168-1923(99)00028-3, 1999.

Ruffault, J., Martin-StPaul, N.K., Rambal, S. et Mouillot, F.: Differential regional responses in drought length, intensity and timing to recent climate changes in a Mediterranean forested ecosystem. *Climatic Change*, 117, 103–117, https://doi.org/10.1007/s10584-012-0559-5, 2013.

Ruffault, J., Pimont, F., Cochard, H., Dupuy, J.-L., and Martin-StPaul, N.: SurEau-Ecos v2.0: a trait-based plant hydraulics model for simulations of plant water status and drought-induced mortality at the ecosystem level, *Geosci. Model Dev.*, 15, 5593–5626, https://doi.org/10.5194/gmd-15-5593-2022, 2022.

Ruffault, J., Limousin, J-.M., Pimont, F., Dupuy, J-.L., De Cáceres, M., Cochard, H., Mouillot, F., Blackman, C.J., Torres-Ruiz, J.M., Parsons, R.A., Moreno, M., Delzon, S., Jansen, S., Olioso, A., Choat, B. and Martin-StPaul, N.: Plant hydraulic modelling of leaf and canopy fuel moisture content reveals increasing vulnerability of a Mediterranean forest to wildfires under extreme drought. *New Phytologist*, 237, 4, 1256-1269, https://doi.org/10.1111/nph.18614, 2023.

Spitters, C.J.T., Toussaint, H.A.J.M., and Goudriaan, J.: Separating the diffuse and direct component of global radiation and its implications for modeling canopy photosynthesis Part I. Components of incoming radiation. *Agr. and Forest Met.*, 38(1-3), 217-229, https://doi.org/10.1016/0168-1923(86)90060-2, 1986.

Shuttle Radar Topography Mission (SRTM): 1 Arc-Second Global (2013). https://doi.org/10.5066/F7PR7TFT (Downloaded on https://earthexplorer.usgs.gov/ the 15-10-2021), 2013.

Stéfanon, M., Martin-StPaul, N. K., Leadley, P., Bastin, S., Dell'Aquila, A., Drobinski, P., and Gallardo, C.: Testing climate models using an impact model: What are the advantages? *Climatic Change*, 131(4), 649–661, https://doi.org/10.1007/s10584-015-1412-4, 2015.

Tappeiner, U., Tasser, E. and Tappeiner, G.: Modelling vegetation patterns using natural and anthropogenic influence factors: preliminary experience with a GIS based model applied to an Alpine area. *Ecological Modelling*, 113(1-3): 225-237, https://doi.org/10.1016/S0304-3800(98)00145-8, 1998.

Zimmermann, N.E. and Kienast, F.: Predictive mapping of alpine grasslands in Switzerland: Species versus community approach. *Journal of Vegetation Science*, 10(4): 469-482, https://doi.org/10.2307/3237182, 1999.